Multi-walled carbon nanotube–Al2O3 composites: Covalent or non-covalent functionalization for mechanical reinforcement

Anne Kasperski, Alicia Weibel, Claude Estournès, Christophe Laurent, Alain Peigney

Multi-walled carbon nanotube–Al_2O_3 composites: Covalent or non-covalent functionalization for mechanical reinforcement

A. Kasperski, A. Weibel,* C. Estournès, Ch. Laurent and A. Peigney

Université de Toulouse, Institut Carnot CIRIMAT, UMR CNRS-UPS-INP 5085, Université Paul-Sabatier, 118 route de Narbonne, 31062 Toulouse cedex 9, France

Multi-walled carbon nanotube–Al_2O_3 composites are prepared using carbon nanotubes (8 walls, 1.5 μm long or 20 walls, 10 μm long) previously submitted to either covalent or non-covalent functionalization. High-energy sonication mixing, freeze-drying and spark plasma sintering lead to dense composites. The shorter CNTs are better dispersed than the longer ones, whatever the functionalization. Crack-bridging by CNTs is evidenced only when non-covalent functionalization is used and is correlated with a high fracture toughness for composites with the longer CNTs.

Keywords: Ceramic matrix composites, Alumina; Carbon nanotubes; Microstructure; Toughness

Carbon nanotube (CNT)–ceramic composites have been studied for about 15 years, the key objective being to increase the fracture toughness compared to the corresponding ceramic [1–2]. Many reports are related to CNT–Al_2O_3 composites. Most authors prefer to use multi-walled CNTs (MWCNTs), which are less prone to damage during the preparation process than single- and double-walled CNTs, and also are cheaper. However, their main characteristics (internal and external diameters, number of walls, length and defect proportion) vary greatly from one study to the other, which can result in large variations in the microstructure and properties of the composite. In particular, the MWCNT/ceramic interface area, which depends on both external diameter and length, is one of the key parameters in the toughening mechanisms, as in the case of micrometric fibre–ceramic composites. Moreover, differences in number of walls and length induce different amounts of MWCNTs for a given carbon content present in the composite [3]. Amounts that are too low or too high result in a poor degree of homogeneity of the MWCNT distribution in the composite. MWCNT characteristics also affect their ability to be dispersed and stabilized in a liquid medium, generally water, prior to the preparation of the MWCNT–ceramic powder, by a commonly used colloidal process [1,2]. The functionalization of the MWCNTs is one of the key steps towards stabilization of the suspension [4]. Both covalent and non-covalent functionalization have been investigated, but the superiority of the latter method, which is less prone to induce damage to the CNTs, has not been clearly established because of the variety of MWCNTs used in the preparations [1,2] and the contested validity of some measurements of the fracture toughness [5,6]. Therefore, in this work, we investigate the influence of the functionalization type on the microstructure, mechanical properties and possible reinforcement mechanisms for MWCNT–Al_2O_3 composites prepared by colloidal mixing, freeze-drying and spark plasma sintering (SPS).

Two kinds of MWCNTs were used for this study. The samples, designated 8WCNT (Nanocyl, Belgium) and 20WCNT (Nanothinx, Greece), have been studied in detail elsewhere [7]. For the 8WCNT sample, CNTs with 8 walls are dominant (30%), with CNTs with 7 and 9 walls (both 16%) being the next most abundant species. The average number of walls (N) is 8.5, which was rounded down to 8 (hence the codename). The CNT length is less than 1.5 μm (supplier data), the average external diameter (d_{ext}) is 10.2 nm and the aspect ratio is around 150. For the 20WCNT sample, the number of walls varies widely, with most being within the range 8–37; CNTs with 17 walls are dominant, but only slightly (at only 10%). $N = 19.8$, which was rounded up to 20. The CNT length is over 10 μm (supplier data), $d_{ext} = 19.6$ nm and the aspect ratio is around 500. For

* Corresponding author. Tel.: +33 0561556175; fax: +33 0561556163; e-mail: weibel@chimie.ups-tlse.fr

http://dx.doi.org/10.1016/j.scriptamat.2013.11.015

both samples, the MWCNTs are not bundled and most MWCNTs present important structural defects, such as kinks, incomplete walls, a bamboo-like structure and variations in diameter along the length. The MWCNT samples were divided into two batches, which were submitted to a covalent or non-covalent functionalization treatment. For covalent functionalization, the MWCNTs were poured into a nitric acid aqueous solution (3 mol l^{-1}) using 1 mg of CNT per ml of solution. After refluxing overnight (130 °C, magnetic stirring), the suspension was neutralized, filtered and redispersed (ultrasonic bath, 80 W, 15 min) in an NaOH aqueous solution (4 mol l^{-1}) in order to remove any disorganized carbon. After neutralization and filtration, the covalent-functionalized MWCNTs obtained were dispersed again in deionized water (Vibra Cell 75042 sonotrode, 500 W operated at 30% power, with 5:5 s on:off pulses, 15 min), yielding a stable suspension (2.5 g l^{-1}) as required for the study. For non-covalent functionalization, the CNTs were dispersed (sonotrode, 30 min) in an aqueous solution of gum arabic (GA), a water-soluble polysaccharide, using the same concentration of 1 g l^{-1} for both CNT and GA.

A commercial α-Al_2O_3 powder (TAIMEI Chemicals Co. Ltd., 99.99% purity, average primary grain size 140 nm) was used for the preparation (15 min sonication and 1 h mechanical stirring) of a suspension in an aqueous solution adjusted to pH 12 by the addition of ammonia [8,9]. The CNT suspension was then poured into the alumina suspension (30 min sonication under mechanical stirring) and the vessel was immersed in liquid N_2 until freezing, whereupon it was freeze-dried (Christ alpha 2–4 LD, Bioblock Scientific) at −84 °C for 48 h in a primary vacuum (12 Pa) [10,11]. Four CNT–Al_2O_3 composite powders were prepared, labelled 8C, 20C, 8NC and 20NC (with 8 and 20 reflecting the average number of walls of the CNTs and C and NC reflecting covalent and non-covalent functionalization, respectively). The CNT suspension volume required to obtain a 2 wt.% carbon content in the composite powder, for the 8WCNTs or the 20WCNTs, was determined from calculations using the CNT density chart [3]. The carbon content (Table 1) in the powders was measured by flash combustion. It corresponds solely to CNTs for the 8C and 20C samples. For the 8NC and 20NC samples, the carbon present in GA (determined by TGA under air) was subtracted to the flash-combustion measured values to obtain the carbon content corresponding to CNTs. All values are slightly lower than 2 wt.% and the corresponding volume fractions of CNTs (Table 1) are in the range 3.0–3.8 vol.%.

From each powder, two pellets were prepared by SPS (Dr. Sinter 2080, SPS Syntex Inc., Japan). First, green samples were prepared by compacting the powders in a stainless steel die (inner diameter 20 mm) under a uniaxial pressure of 200 MPa. The greens were loaded into a 20 mm inner diameter graphite die. A sheet of graphitic paper was placed between the punch and the sample as well as between the die and the sample for easy removal. The SPS treatment was performed in vacuum (residual cell pressure <3 Pa). A pulse pattern of 12 current pulses followed by 2 periods of zero current was used. The temperature was controlled using a thermocouple placed in a little hole (5 mm deep) located on the outer surface of the die. Heating rates of 150 and 100 °C min^{-1} were used from room temperature to 650 °C and from 650 to 1350 °C, respectively, where a dwell (6 or 11 min) was applied. For the 8C and 20C samples, a uniaxial charge (corresponding to 150 MPa) was gradually applied within the first minute of the dwell, maintained for a further 5 min and gradually released during the cooling down to room temperature (100 °C min^{-1}). For the 8NC and 20NC samples, a 5 min dwell time was added at 1350 °C before the application of the uniaxial load, to ensure the decomposition of GA in the still porous composite (i.e. the total dwell time was 11 min). For the sake of comparison, an Al_2O_3 sample was prepared by SPS (using the as-received powder) at only 1150 °C (6 min dwell), in order to obtain a dense sample with an average alumina grain size similar to that of the alumina matrix in CNT–Al_2O_3 composites [12].

The sintered specimens were in the form of pellets 20 mm in diameter and about 2 mm thick. The density was determined by the Archimedes method after removal of the graphitic surface contamination layer by light polishing. The relative densities, calculated using 1.8 g cm^{-3} for the 8WCNTs and 2.1 g cm^{-3} for the 20WCNTs [3], are about 100% for Al_2O_3, 8C and 20C and in the range 97–98% for 8NC and 20NC, probably because some porosity produced by the decomposition of GA could not be fully resorbed during sintering.

Raman spectroscopy analyses (Jobin–Yvon LabRAM HR800, laser excitation at 632.82 nm) were performed at different steps in the study. The ratio between the intensities of the D band and the G band (I_D/I_G, Table 2) was calculated from the spectra (not shown). A higher ratio is generally attributed to the presence of more structural defects in the CNTs. There is not much change in the I_D/I_G ratio for the 8WCNTs (or the 20WCNTs), whether raw, covalent-functionalized or in the composite powder, showing no drastic

Table 1. Carbon content (corresponding to CNTs, i.e. corrected for carbon present in gum arabic for 8NC and 20NC) in the composite powders (C_n), alumina average grain size (G), electrical conductivity (σ_e),Vickers microhardness (H_V), bending fracture strength (σ_f), SENB fracture toughness (K_{Ic}) of alumina and CNT–alumina composites (standard deviations are indicated for the mechanical properties).

Specimen	C_n		G	σ_e	H_V	σ_f	K_{Ic}
	(wt.%)	(vol.%)	(nm)	(S.cm^{-1})	(GPa)	(MPa)	(MPa.$m^{1/2}$)
Al_2O_3	0	0	320	–	21.3 ± 1.5	413 ± 84	5.4 ± 1.4
8C	1.8	3.8	170	1.0	19.0 ± 1.6	456 ± 61	4.1 ± 0.5
8NC	1.4	3.0	170	1.7	18.4 ± 1.3	468 ± 62	4.2 ± 0.9
20C	1.7	3.2	300	0.32	19.8 ± 1.1	377 ± 55	3.8 ± 0.6
20NC	1.9	3.6	330	0.14	17.8 ± 3.4	313 ± 68	5.2 ± 2.3

Table 2. Ratio between the intensities of the D band and the G band (I_D/I_G) calculated from the Raman spectra for the CNTs at different steps in the study: raw, covalent-functionalized, in the composite powders and in the dense composites.

Step	8C	8NC	20C	20NC
Raw	1.86	1.86	1.27	1.27
Covalently functionalized	1.88	–	1.42	–
In composite powder	1.77	1.85	1.28	1.41
In dense composite	1.28	1.38	1.10	1.19

deterioration to the structure of CNTs – which, as noted above, are nevertheless quite defective. By contrast, the I_D/I_G ratio for the CNTs in the dense composites is slightly lower, probably indicating the annealing of some defects involving sp^3 carbon by the SPS treatment at 1350 °C.

The fracture surfaces of the pellets (Fig. 1) were observed by field emission gun scanning electron microscopy (FESEM; JEOL JSM 6700F). For all samples, the fracture mode is intergranular. The average alumina grain size (G, Table 1) was determined from such images by the mean linear intercept method. For the Al_2O_3 sample (Fig. 1a), $G = 320$ nm. For 8C (not shown) and 8NC (Fig. 1b), it is significantly lower (170 nm), in agreement with earlier results showing that the matrix grain growth is inhibited by the CNTs [1–2]. Indeed, CNTs that do not appear to have been damaged are well distributed at the matrix grain boundaries, without forming agglomerates. For 20C and 20NC, the matrix grain size is about 300–330 nm (Fig. 1c and d), reflecting the lesser influence of the 20WCNTs due to their lower number and lower total length (for the same carbon content, the number of 20WCNTs in the sample and their total length are 25 and 4 times lower, respectively, than for 8WCNTs), and their less homogeneous distribution. Indeed, CNTs and CNT imprints are observed (arrowed in Fig. 1c and d) at most alumina grain boundaries, though some CNT agglomerates, up to 30 μm long, are also evident. This could, in turn, reflect that 20WCNTs are more difficult to disperse than 8WCNTs because of their higher aspect ratio (500 vs. 150). Note that grain-growth inhibition is still active, because the average grain size is similar to that of Al_2O_3 despite the higher sintering temperature (1350 vs. 1150 °C).

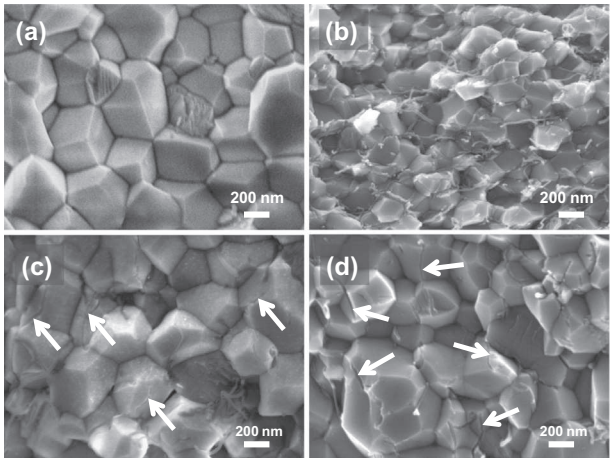

Figure 1. FESEM images of the fracture surface of the Al_2O_3 sample (a) and the 8NC (b), 20C (c) and 20NC (d) composites.

Note also that neither the average grain size nor the CNT distribution depends on the functionalization method.

The pellets were polished down to 1 μm using diamond slurries. The electrical conductivity was measured at room temperature with direct currents applied to ($1.8 \times 1.8 \times 1.5$ mm^3) specimens parallel to their length, i.e. perpendicular to the pressing axis. The current densities used were lower than 160 mA cm^{-2} (Keithley 2400). All composites present an electrical conductivity of at least 0.1 S cm^{-1} (σ_e, Table 1), reflecting that the carbon contents are higher than the percolation threshold measured on similar composites [1–2]. However, the values are higher for 8C and 8NC than for 20C and 20NC, reflecting the higher CNT number and total length, and the better distribution of the 8WCNTs, as noted above. The electrical conductivity for 8NC (1.7 S cm^{-1}) is amongst the higher values reported for well-densified MWCNT–Al_2O_3 composites with a similar CNT content [1–2], slightly higher than that (1.3 S cm^{-1}) reported by Inam et al. [12], which confirms the high degree of homogeneity of the CNT distribution. The lower electrical conductivity for 8C (1.0 S cm^{-1}), despite a similar CNT distribution could indicate that the CNTs sustained some structural damage during the covalent functionalization.

The indentation tests (300 g for 10 s in air at room temperature) were performed on the polished surface of eight specimens by loading with a Vickers indenter (Shimadzu HMV 2000). The corresponding diagonals of the indentation were measured using an optical microscope attached to the indenter. The calculated microhardness values (Table 1) are the average of 10 measurements. The Vickers microhardness of the composites (17.8–19.8 GPa) is lower than that of the Al_2O_3 sample (21.3 GPa), in good agreement with earlier results [13,14]. The transverse fracture strength (σ_f) was measured by the three-point bending method on eight specimens with dimensions of about $1.8 \times 1.8 \times 18$ mm^3. The fracture toughness (K_{Ic}) was measured by the SENB method on similar specimens notched with a diamond wire 0.17 mm in diameter and calculated using a calibration factor [15]. For each composition, eight samples were tested for σ_f and eight for K_{Ic}. The cross-head speed was fixed at 0.1 mm min^{-1}. No composite shows both a higher fracture strength and a higher fracture toughness than Al_2O_3 (Table 1). The 8C and 8NC samples have a slightly higher fracture strength (456–468 vs. 413 MPa) but a lower toughness (4.1–4.2 vs. 5.4 MPa.m$^{1/2}$), which could be correlated with the smaller alumina grain size (170 vs. 320 nm) [16], without any direct effect of the CNTs being clearly observed. For 20C, both σ_f and K_{Ic} are lower than for Al_2O_3 despite a similar grain size. By contrast, 20NC also shows a lower σ_f, though K_{Ic} is similar to that for Al_2O_3 (5.2 vs. 5.4 MPa.m$^{1/2}$). The presence of CNT agglomerates in 20C and 20NC could account for the low fracture strength because the larger agglomerates (up to 30 μm in length) have a size comparable to the critical-flaw size, even taking into account the higher K_{Ic} for 20NC. Indeed, these agglomerates are very porous and easily deformable, presenting the same behavior as large pores.

To investigate the possible mechanisms of crack deflection or crack bridging by the MWCNTs in more detail, Vickers indentations were performed on the polished surfaces of the composites using a high enough load (2 kg) to produce cracks, which were observed by FESEM (Fig. 2). For 8C (Fig. 2a) and 20C (Fig. 2b), some CNTs are observed on the edges of the crack, but not bridging the crack. In contrast, large-scale crack bridging is observed for 8NC (Fig. 2c) and 20NC (Fig. 2d). This could reveal that covalent functionalization weakens the MWCNTs whereas non-covalent functionalization does not.

As discussed elsewhere [17,18], the crack propagation by decohesion at the grain boundaries causes the CNTs, which are mechanically locked by adjacent ceramic grains, to become progressively unfolded and taut, one by one, as the crack widens, thus ensuring some load transfer. At a certain point, all the CNTs which are thus unfolded do bridge the crack. Some bridging CNTs are broken, therefore absorbing a fraction of the fracture energy. The elastic deformation energy absorbed by one CNT for unfolding is weak but the cumulated energy necessary for the fracture of all bridging CNTs is much higher and this would thus likely limit the crack propagation. Moreover, we observe that crack bridging CNTs are mostly perpendicular to the crack direction (Fig 2c and d), which could correspond to pull-out, whereas oblique crack bridging could correspond to unfolding. Thus, pulling-out of CNTs could also limit the crack propagation. The poor toughness (4.2 $MPa.m^{1/2}$) for 8NC, despite crack bridging, could reflect that the 8WCNTs are short and have a low aspect ratio, and thus that the mechanical locking by the alumina grains would not extend very far, allowing for pull-out with only a low tensile stress. For the much longer 20WCNTs, which also have a much higher aspect ratio, the pull-out critical stress would be sufficiently high to lead to crack bridging, thus bridging by CNTs and pulling-out of CNTs could both contribute to the reinforcement.

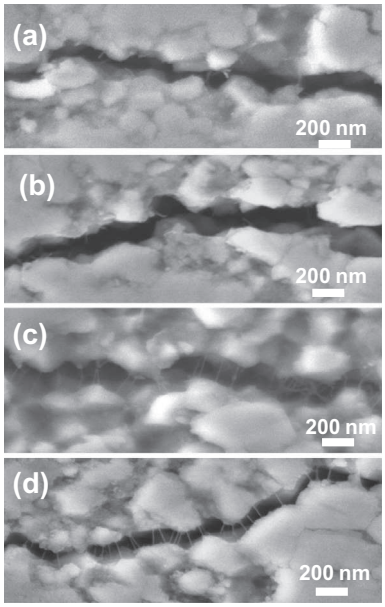

Figure 2. FESEM images of cracks made by Vickers indentation using a high load (2 kg) on the 8C (a), 20C (b), 8NC (c) and 20NC (d) composites.

In conclusion, this work shows that MWCNTs (8 walls, 1.5 μm long or 20 walls, 10 μm long), with prior covalent functionalization, are not able to provide any crack bridging in the corresponding Al_2O_3-matrix composites, probably because the chemical treatment was detrimental to their mechanical properties, which is correlated with low fracture toughness. In contrast, the non-covalent functionalization (here performed with gum arabic) preserves the mechanical properties of the MWCNTs, thus allowing for crack bridging on a large scale in the corresponding composites. Moreover, it is shown that, in order for this to provide toughening, long MWCNTs (>10 μm) are to be preferred to shorter ones (<1.5 μm), although they are more difficult to disperse homogeneously because they permit the establishment of sufficiently long mechanical interlocking of the CNTs by the matrix grains.

The FESEM observations were performed at TEMSCAN, the "Service Commun de Microscopie Electronique à Transmission", Université Paul Sabatier, Toulouse. The authors thank G. Chevallier for assistance with the SPS, which was performed at the Plateforme Nationale CNRS de Frittage Flash (PNF^2, Toulouse).

[1] J. Cho, A.R. Boccaccini, M.S.P. Shaffer, J. Mater. Sci. 44 (2009) 1934.
[2] E. Zapata-Solvas, D. Gomez-Garcia, A. Dominguez-Rodriguez, J. Eur. Ceram. Soc. 32 (2012) 3001.
[3] C. Laurent, E. Flahaut, A. Peigney, Carbon 48 (2010) 2994.
[4] M. Estili, A. Kawasaki, H. Sakamoto, Y. Mekuchi, M. Kuno, T. Tsukada, Acta Mater. 56 (2008) 4070.
[5] B.W. Sheldon, W.A. Curtin, Nat. Mater. 3 (2004) 505.
[6] X.T. Wang, N.P. Padture, H. Tanaka, Nat. Mater. 3 (2004) 539.
[7] C. Guiderdoni, E. Pavlenko, V. Turq, A. Weibel, P. Puech, C. Estournes, A. Peigney, W. Bacsa, C. Laurent, Carbon 58 (2013) 185.
[8] S.C. Zhang, W.G. Fahrenholtz, G.E. Hilmas, E.J. Yadlowsky, J. Eur. Ceram. Soc. 30 (2010) 1373.
[9] R. Poyato, A.l. Vasiliev, N.P. Padture, H. Tanaka, T. Nishimura, Nanotechnology 17 (2006) 1770.
[10] M. Poorteman, M. Traianidis, G. Bister, F. Cambier, J. Eur. Ceram. Soc. 29 (2009) 669.
[11] M. Belmonte, C. Valles, W.K. Maser, A.M. Benito, M.T. Martinez, P. Miranzo, M.I. Osendi, J. Nanosci. Nanotechnol. 9 (2009) 6164.
[12] J.G. Santanach, A. Weibel, C. Estournes, Q. Yang, C. Laurent, A. Peigney, Acta Mater. 59 (2011) 1400.
[13] G. Yamamoto, M. Omori, T. Hashida, H. Kimura, Nanotechnology 19 (2008).
[14] S.W. Kim, W.S. Chung, K.S. Sohn, C.Y. Son, S. Lee, Metall. Mater. Trans. A 41A (2010) 380.
[15] W.F. Brown, J.E. Srawley, ASTM Special Technical Publication, ASTM, Philadelphia, PA, 1966.
[16] D. Kovar, S.J. Bennison, M.J. Readey, Acta Mater. 48 (2000) 565.
[17] A. Kasperski, A. Weibel, C. Estournes, C. Laurent, A. Peigney, Carbon 53 (2013) 62.
[18] A. Peigney, F.l. Garcia, C. Estournes, A. Weibel, C. Laurent, Carbon 48 (2010) (1952).